Pressure anomalies from the January 2022 Hunga Tonga-Hunga Ha'apai eruption

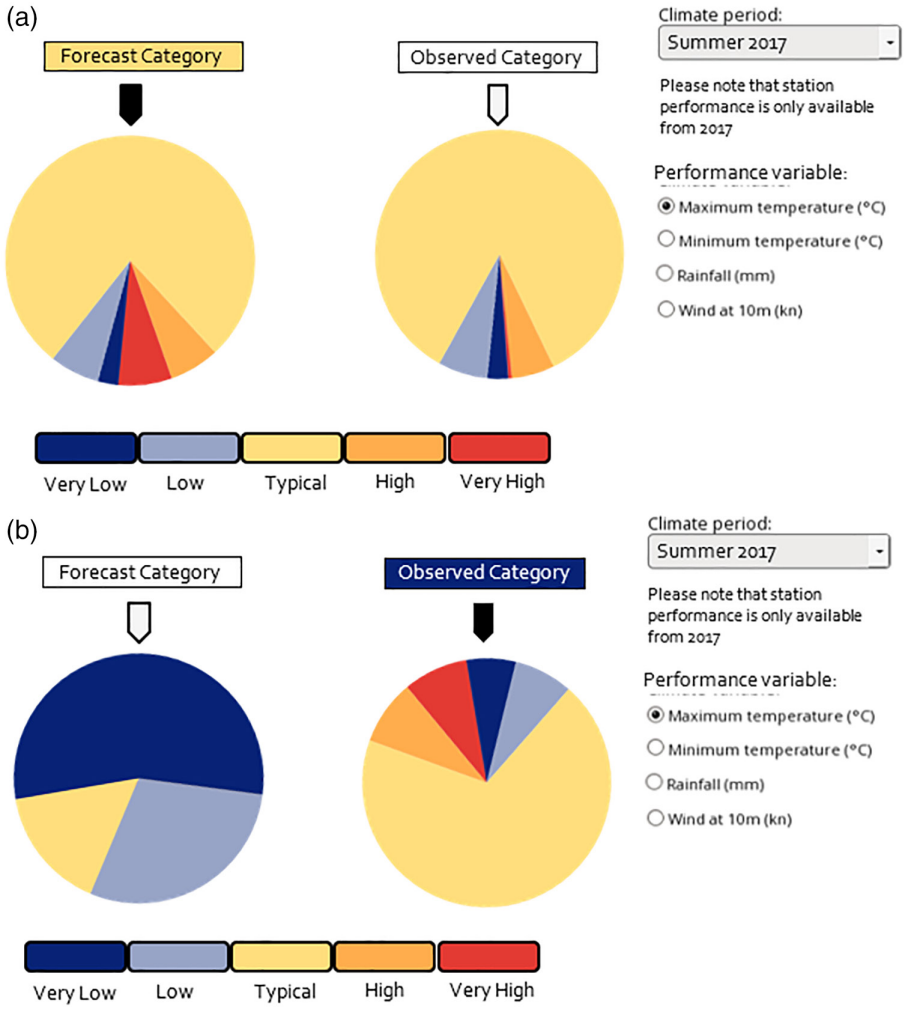

Figure 9. A colour-based, nonnumeric, graphical presentation of the performance of day 1 forecasts at all UK observation sites that appeared on the Met Office App during the summer of 2017. (a) Displays the distribution of observed categories when 'typical' temperatures were forecast and (b) displays the distribution of forecast categories when 'very low' temperatures were observed.

bers, both deterministic and probabilistic forecast performance in simple, practical and easy-to-understand ways for single sites, districts, regions or even the whole country. If you have any thoughts on the use of climatology to present weather information the author would be delighted to hear from you.

References

Cecchini M, **Warin L**. 2016. Impact of food labelling systems on food choices and eating behaviours: a systematic review and meta-analysis of randomized studies. *Obes. Rev.* **17**(3): 201–210.

Chan EY. 2018. Climate change is the world's greatest threat – in Celsius or Fahrenheit? *J. Environ. Psychol.* **60**: 21–28.

Hygen HO, **Schuler DV**, **Midtdal A *et al***. 2017, 2017. *A Lucky Spin, EMS Annual Meeting Abstracts*, Vol. 14, pp EMS2017–EMS2583. https://meetingorganizer.copernicus.org/EMS2017/EMS2017-583.pdf

Jolliffe IT, **Stephenson DB**. 2012. *Forecast Verification: A Practitioner's Guide in Atmospheric Science*. John Wiley & Sons: Chichester, UK.

Lin TP. 2009. Thermal perception, adaptation and attendance in a public square in hot and humid regions. *Build. Environ.* **42**: 2017–2026.

Lin T, **Matzarakis A**. 2008. Tourism climate and thermal comfort in Sun Moon Lake, Taiwan. *Int. J. Biometeorol.* **52**: 281–290.

Lin TP, **de Dear R**, **Hwang RL**. 2010. Effect of thermal adaptation on seasonal outdoor thermal comfort. *Int. J. Climatol.* **31**(2): 302–312.

Rutty M, **Scott D**. 2013. Differential climate preferences of international beach tourists. *Clim. Res.* **57**: 259–269.

Rutty M, **Scott D**. 2015. Bioclimatic comfort and the thermal perceptions and preferences of beach tourists. *Int. J. Biometeorol.* **59**: 37–45.

Sharpe M, **Stewart E**. 2019. Verification of post-processed summer temperature forecasts at UK sites using observed climate-based thresholds. *Wea. Forecast.* **34**: 715–730.

Temple NJ, **Fraser J**. 2014. Food labels: a critical assessment. *Nutrition* **30**(3): 257–260.

Correspondence to: M. Sharpe
michael.sharpe@metoffice.gov.uk

doi: 10.1002/wea.3901

Pressure anomalies from the January 2022 Hunga Tonga-Hunga Ha'apai eruption

Giles Harrison
Department of Meteorology, University of Reading, Reading, UK

The major eruption of the Hunga Tonga-Hunga Ha'apai volcano at 0410 UTC on 15 January 2022 following lesser activity in the previous days, was so substantial that it sent a shock wave propagating around the globe. As was the case for the eruption of Krakatoa in August 1883 (Symons, 1888), the initial pressure changes associated with the shock wave were so large that they were detected around the world with barometers in routine meteorological use, and are well within the capability of inexpensive digital sensors (Harrison, 2021) bringing the prospect of a considerable amount of high quality data.

The Tonga pressure wave propagated outwards from the volcano, leading to its first appearance in the United Kingdom around 1800 UTC on 15 January having passed over the North Pole, with a sec-

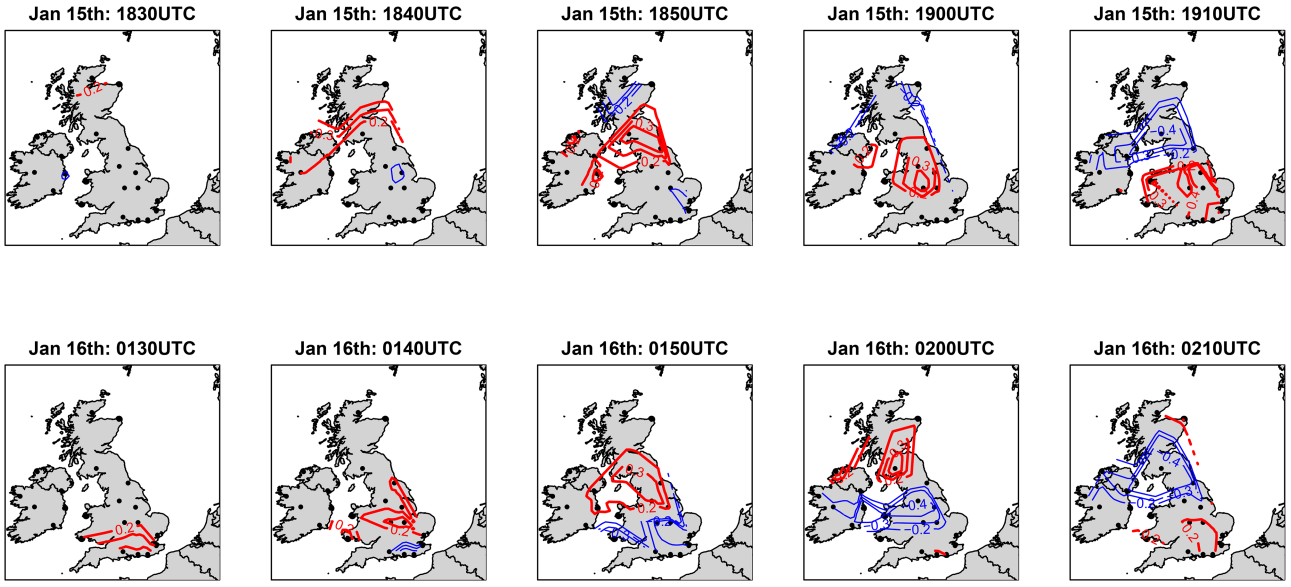

Figure 1. Pressure anomalies in the UK and Ireland during the first (upper row) and second (lower row) pulses from the Tonga eruption. Thick red lines show positive anomalies, and thin blue lines negative anomalies. (Data are 10min values from a representative sample of the pressure-equipped Vaisala roadside network, time-aligned, spline-detrended and spatially contoured in 0.2hPa steps. Site locations used are marked with small dots.)

ond appearance at about 0200 UTC on 16 January via the South Pole route. Figure 1 shows a preliminary analysis of pressure anomalies over the UK from roadside monitoring sensors, as used previously for the 2015 eclipse (Gray and Harrison, 2016). It shows the arrival of the first pressure pulse from the north and propagating southwards, and the second pressure pulse arriving from the south and propagating northwards at a similar speed to the first pulse. Both caused transient pressure anomalies of 0.5 to 1hPa, which were initially positive and then negative, and made more observable by reasonably settled anticyclonic conditions.

At Reading, the first sign of a pressure pulse was at about 1845 UTC, 14.5 hours after the eruption. For the separation between Reading and Tonga of about 16 500km, this corresponds to a wave speed of 315ms^{-1}, which is close to the speed of sound at standard conditions. Figures 2(a) and (b) show the first two pressure pulses considered in Figure 1 arriving at Reading, observed using a Druck DPI140 barometer with ±0.01hPa resolution operating on the vibrating drum principle (Harrison, 2014), sampled at 1s intervals. The pulse shapes are reminiscent of the initial pressure pulses observed following the Krakatoa eruption (Figures 2c and d), with a slow increase to a ragged maximum followed by a rapid descent to a minimum. With the greater resolution present in the modern data, the first pulse at Reading can be seen to be followed by high frequency variability lasting several hours. Compared with the period before the first pulse, greater background variability continued after the second pulse, implying that the atmosphere remained disturbed.

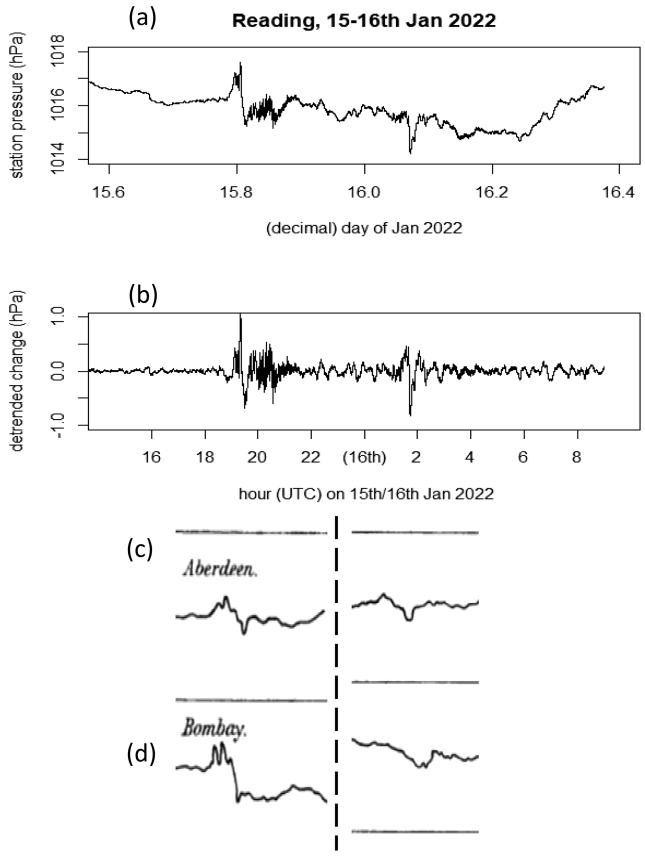

Figure 2. Time series of (a) station pressure from Reading, using 1s sampled data and (b) detrended pressure, using a fitted smoothing spline. Barograms from (c) Aberdeen and (d) Bombay for the first and second pressure pulses from the Krakatoa eruption of August 1883 (from Symons, 1888; no time or pressure axis provided).

As for Krakatoa, pairs of further pulses arrived at Reading with intervals of about 35 to 36 hours from the previous pair of pulses. Numbering the pulses individually, the first and subsequent odd-numbered pulses had initially taken the North Pole route, and the even-numbered pulses the longer South Pole route. Figure 3(a) shows a continuation of the pressure data from Figure 2(a), with the pressure pulses identified in Figure 3(b). For the later pulses, the amplitude decreased, making it dif-

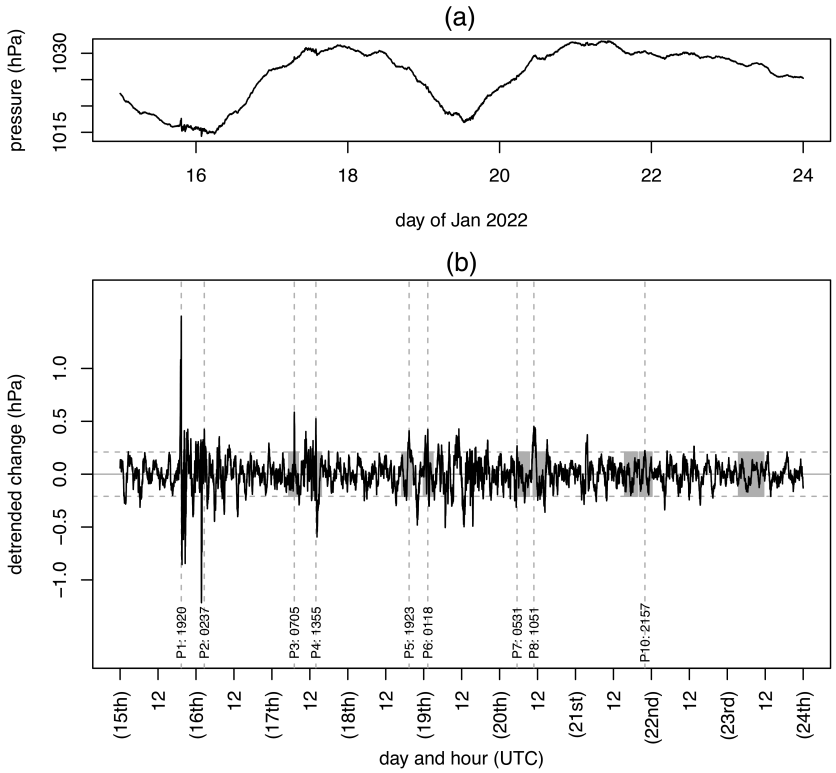

Figure 3. Time series of (a) station pressure from Reading, and (b) detrended pressure, using 1s data, spline detrended. In (b) the pulses likely to be from the Tonga pressure wave are marked with vertical dashed lines, numbered and timed. These are identified as local maxima exceeding two standard deviations of the pressure fluctuations before the first pulse's arrival (horizontal dashed lines), and occuring within the time window estimated from the previous pulse (grey blocks).

Table 1

Pressure wave pulse timing and intervals at Reading

Pulse number	*Day of January 2022*	*Time of maximum (UTC)*	*Interval from previous odd or even pulse (hours)*	*Transit speed (ms^{-1})*
P1	15	1920		
P2	16	0237		
P3	17	0735	35.7	311
P4	17	1355	35.3	315
P5	18	1923	36.3	306
P6	19	0118	35.4	314

Earth radius assumed R_E = 6371km.

ficult to identify the pulses uniquely. The approach adopted was a combination of expected timing and a comparison with the typical undisturbed variability – found as two standard deviations – in the pressure fluctuations before the first pulse. Subsequent maxima in pressure fluctuations which both (1) exceeded this variability, and (2) occurred in a time window estimated from the previous pulse, were regarded as contenders for having been generated by the returning pressure wave. On this basis, six pulses (P1 to P6) were reasonably straightforwardly identified. However, changed background variability through passage of a weak front gives less confidence in identifying pulses 7 and 8. Pulse 10 only marginally meets the criteria applied, the detailed application of which and the choices made in the detrending method used then become more important. Further analysis using pattern matching (as for the pressure pulse from the 2005 Buncefield explosion, Mather *et al*. (2007)), or spectral methods, may improve on this.

Table 1 summarises the timing information obtained for the first six pulses, using the time of the pulse maximum in each case. The mean speeds of the odd pulses (North Pole route initially) and evenly numbered pulses are 309ms^{-1} and 314ms^{-1} respectively. A similar difference was found for pulse pairs in the Krakatoa event, which was attributed by Symons (1888) to an assisting or opposing contribution of the prevailing winds globally. The 5ms^{-1} difference observed is consistent with this.

The passage of a large pressure disturbance might be expected to generate additional local atmospheric changes associated with fluid motion. Whilst the pressure was sampled with a rapid response instrument (Figure 4a), standard meteorological instruments respond less rapidly, so a straightforward comparison is difficult. The Vaisala CL31 laser ceilometer operating at Reading, however, provides one minute samples of cloud base height. During the passage of the first pressure pulse on 15 January, low stratus cloud was present, with a mean cloud base of 1200m between 1700 and 2300 UTC. Removing slow changes in the mean cloud base using a spline method, the variability generated in the cloud base during the passage of the pressure wave becomes apparent (Figure 4b). The sudden rise in the cloud base height just before 2000 UTC was also observed as a decrease in both the long-wave down flux and the surface potential gradient (which responds to charge at the cloud base changing its position), and an increase in the surface air temperature sensed by an aspirated thermometer able to respond within one minute.

The Krakatoa pressure wave was a defining event in atmospheric science, due to its detection in the early international measurement network through the impressively thorough activities of the Krakatoa committee. The 2022 Hunga Tonga-Hunga Ha'apai pressure wave, which has been exquisitely sampled by modern instruments and satellite imagery in a way inconceivable in 1883, is likely to prove equally valuable.

Acknowledgements

I am grateful to David Bullock of Vaisala for providing the roadside station data used for Figure 1.

Data availability statement

Data used are available at: https://doi.org/10.17864/1947.000354.

References

Gray SL, **Harrison RG**. 2016. Eclipse-induced wind changes over the British Isles on the 20 March 2015. *Phil. Trans. R. Soc. A* **374**: 20150224

Harrison RG. 2014. *Meteorological Measurements and Instrumentation*. Wiley: Chichester, UK.

Harrison RG. 2021. Make your own Met measurements: build a digital barometer for about £10. *Weather* **76**(2): 45–47.

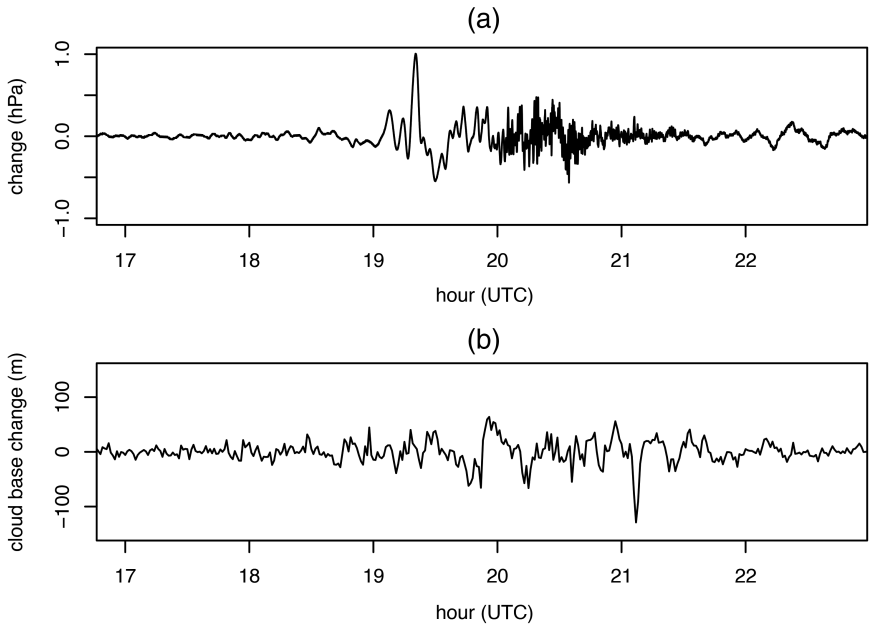

Figure 4. Detrended time series of (a) surface atmospheric pressure and (b) cloud base height at Reading on 15 January 2022.

Mather TA, **Harrison RG**, **Tsanev VI** ***et al***. 2007. Observations of the plume generated by the December 2005 oil depot explosions and prolonged fire at Buncefield (Hertfordshire, UK) and associated atmospheric changes. *Proc. R. Soc. A* **463**: 1153–1177.

Symons GJ (ed). 1888. *Report of the Krakatoa Committee of the Royal Society*. Trübner & Company: London, UK.

Correspondence to: G. Harrison

r.g.harrison@reading.ac.uk

doi: 10.1002/wea.4170

Insights

Solar energy and weather

Eadaoin Doddy Clarke and Conor Sweeney

School of Mathematics and Statistics, UCD, Dublin 4, Ireland

What is solar energy?

Countries are transitioning to a net-zero emissions focus for future electricity supply. The majority of the technologies used to achieve this are dependent on the weather, such as wind and solar farms. Consequently the weather will play a substantial role in the energy produced from these technologies. One type of solar technology involves generating electricity from solar photovoltaic (PV) panels. The Sun emits energy in the form of solar radiation, approximately 1361Wm^{-2} annually at the top of the atmosphere, normal to the incoming rays. About 30% of this is reflected back to space with about 70% reaching the Earth's surface. This can be captured and turned into electricity, using PV panels. These convert sunlight into electricity through the process of a solar cell absorbing solar radiation to excite electrons into higher energy states.

How much solar energy is generated?

PV output is generated by shining light on a substance and creating a voltage. Power generation fluctuates with the variation of in-plane irradiance. PV panels are situated with optimised inclination angles to achieve maximum power generation over the year. The intensity of solar radiation depends on a number of factors including geographic location, season and time of day. Solar radiation input arrives in the form of both direct beam and diffuse radiation (Figure 1). Passing clouds are the main cause of blocking light from reaching the panels. The concentration of aerosols, water vapour and ozone in the atmosphere determine how much solar radiation is absorbed, scattered or reflected before reaching the ground. This is called diffuse radiation. When the Sun is lower in the sky, rays travel through a greater path length of the atmosphere and they become more scattered and diffuse, resulting in a greater component of diffuse radiation. Seasons control the amount of sunlight on any particular day, with up to 18h in summer and as little as 8h in winter around Ireland and the United Kingdom. During winter, the Sun is also lower in the sky. The diurnal cycle of sunlight means the greatest amount of solar energy is generated around solar noon and of course, none is generated during night time.

The quantity of energy produced depends on the type of PV module (i.e. the semiconductor material used in the modules), the system set-up (module orientation and tilt angle), along with the prevailing meteorological conditions. PV module efficiency is primarily influenced by the amount of solar radiation that arrives at the PV modules and the temperature of the PV modules. Module temperature in turn depends on the ambient air temperature, the intensity of the solar radiation and on the cooling effect due to local wind speed and direction. Power output decreases with an increase in module temperature and increases as a non-linear function of solar radiation.

The weather can affect PV output in other, less direct ways. PV panel efficiency decreases with the presence of dust and dirt (which can be washed away by rain or with regular cleaning), or by frost and snow on the solar panels. Beyond the panel itself,